

Article

New Methods for Assessing External Sulfate Attack on Cement-Based Specimens

Othman Omikrine Metalssi ^{1,*} , Marc Quiertant ² , Mike Jabbour ¹ and Véronique Baroghel-Bouny ¹

¹ Laboratoire Matériaux pour une Construction Durable (UMR MCD), University Gustave Eiffel, Cerema, F-77454 Marne-la-Vallée, France; mike.k.jabbour@gmail.com (M.J.); veronique.baroghel-bouny@univ-eiffel.fr (V.B.-B.)

² Laboratoire Expérimentation et Modélisation pour le Génie Civil et Urbain (EMGCU), Materials and Structures (MAST) Department, University Gustave Eiffel, F-77454 Marne-la-Vallée, France; marc.quiertant@univ-eiffel.fr

* Correspondence: othman.omikrine-metalssi@univ-eiffel.fr

Abstract: This paper presents two original methods for monitoring and evaluating concrete specimens/structures affected by external sulfate attack (ESA). The first is a drying method developed to assess the penetration depth of sulfate ions in a concrete structure, as this parameter is a relevant indicator of the progress of the ESA. This method has been specifically designed for on-site investigations. The second experimental method involves the use of optical fibers capable of measuring the swelling response of specimens to ESA in real time. According to the results obtained, these two new methods seem likely to be used to complement or replace traditional methods such as inductively coupled plasma (ICP) for determining the penetration depth of sulfate ions or as extensometers for measuring swelling. These traditional methods (ICP and extensometers) are generally considered painful and time-consuming, whereas, because of its simplicity, the proposed drying method will enable experts to regularly inspect concrete structures and make informed decisions on the measures to be taken to repair or prevent further damage induced by ESA, while the second method appears promising for experimental studies involving the monitoring of a large number of ESA-affected specimens.

Keywords: external sulfate attack; structure monitoring; optical fibers; drying method; cementitious materials



Citation: Omikrine Metalssi, O.; Quiertant, M.; Jabbour, M.; Baroghel-Bouny, V. New Methods for Assessing External Sulfate Attack on Cement-Based Specimens. *Appl. Sci.* **2024**, *14*, 1410. <https://doi.org/10.3390/app14041410>

Academic Editor: Norhisham H. Bakhary

Received: 29 December 2023

Revised: 1 February 2024

Accepted: 2 February 2024

Published: 8 February 2024



Copyright: © 2024 by the authors. Licensee MDPI, Basel, Switzerland. This article is an open access article distributed under the terms and conditions of the Creative Commons Attribution (CC BY) license (<https://creativecommons.org/licenses/by/4.0/>).

1. Introduction

Reducing CO₂ emissions in concrete production is a critical priority for sustainable construction practices. With the rising awareness of environmental impacts, there is a growing demand for innovative technologies and processes that can minimize the carbon footprint of concrete [1,2]. This includes exploring alternative binders such as fly ash, slag, and calcined clays, as well as developing more energy-efficient kiln technologies [3,4]. Additionally, the use of fiber optic technology in structural health monitoring systems for civil engineering infrastructure offers a way to reduce CO₂ emissions. By enabling real-time, remote monitoring of the structural integrity of bridges, buildings, and other critical infrastructure, fiber optic sensors can help identify and address potential structural issues before they become major problems [5]. This proactive approach can lead to more efficient maintenance and repair strategies, ultimately extending the lifespan of infrastructure and reducing the need for energy-intensive construction activities associated with major repairs or replacements. Furthermore, by providing accurate and timely data on structural performance, fiber optic monitoring systems can optimize the use of materials and resources, minimizing the environmental impact of construction and maintenance activities.

Reinforced concrete (RC) structures are susceptible to a variety of destructive processes when exposed to aggressive agents [6,7]. External sulfate attack (ESA) is a significant threat to structures, compromising their durability [8]. During ESA, cement-based materials

undergo a chemical attack resulting in the formation of aluminates due to the ingress of sulfate ions via a transport process [9]. In this regard, ESA appears to be the result of two processes. The first step is the transfer of sulfate ions from the external environment into the cement matrix, followed by the leaching of calcium ions from the cement matrix. There are many parameters that influence this process, including the porosity and permeability of the matrix. Second, the chemical composition of the cementitious material determines the chemical processes involved. Hydrate compounds react with residual anhydrous compounds and sulfate ions during this process. As the two processes coexist, it is imperative to analyze both the physical and chemical aspects of ESA [10,11].

In ESA, pores or cracks are partially or completely filled by expanding products (ettringite, gypsum), resulting in changes in the microstructure, microcracking, and loss of strength [12]. The main cause of microstructural changes in cementitious materials exposed to ESA is the formation of ettringite and/or gypsum within capillary pores and smaller gel pores [10,13,14]. During the early stages of attack, ettringite crystals accumulate in voids. As ESA progresses within the material, the crystals invade smaller capillary and gel pores, causing excessive expansion and damage. For this reason, macroscopic and microscopic evaluation methods appear to be useful in assessing the damage mechanisms associated with ESA [13].

The progress of ESA is influenced by several factors. These factors include the cement's chemical composition, including its tricalcium aluminate (C_3A) content, the presence of minerals, and the water-to-cement ratio. In addition to pH, exposure time, and temperature, other variables such as the type of ions associated with the sulfate ions can also affect the attack and transport process. The physicochemical aspects of ESA and their destructive effects on cementitious materials have been extensively investigated in numerous studies [15–19]. However, few experimental studies have considered the combined effect of exposure conditions, cement type, and water-to-cement ratio on cementitious materials in order to describe the ESA mechanisms on the real exposed structures [20–22].

The assessment of carbonation and chloride diffusion is generally considered easier to conduct on existing structures compared with evaluating ESA for several reasons: Firstly, carbonation and chloride diffusion can be assessed nondestructively using methods such as concrete resistivity, half-cell potential measurements, and chloride ion penetration tests that do not require invasive measures that could damage the structure. In addition, carbonation and chloride diffusion are the two most common causes of concrete deterioration for which there are established test methods. ESA, on the other hand, is much less common, and its assessment often requires more specialized knowledge and techniques. Furthermore, carbonation and chloride diffusion on concrete are generally well understood and documented, making interpretation and action easier. Lastly, identifying carbonation- and chloride-induced corrosion on concrete surfaces is relatively straightforward with simple color indicators (phenolphthalein for carbonation and silver nitrate for chloride diffusion). However, identifying the specific mechanisms and manifestations of ESA may require additional expertise.

To sum up, the assessment of ESA on structures is challenging for several reasons. ESA is complex and progressive in nature, making it difficult to detect and evaluate [23–25]. Laboratory analysis is often required to confirm the presence of sulfates. Furthermore, as discussed above, the effects of ESA vary depending on several factors including environmental conditions [26]. In addition, ESA can be difficult to distinguish from other types of degradation [13]. Expertise and continuous monitoring are then essential in cases of ESA [27]. Only a rigorous analysis can enable an accurate assessment of the damage caused by the ESA. According to survey results, repair recommendations and ongoing damage monitoring can be provided to ensure that structures are maintained in a safe and functional condition, thereby reducing the risk of structural failure.

The inductively coupled plasma (ICP) test is considered one of the most reliable methods for measuring sulfate profiles in concrete [10,13,28,29]. However, this method can have some difficulties in application. In addition to its high cost, sample preparation

is a complex process. Samples are often extracted from sulfates by dissolving them in a strong acid. It is important to note that this dissolution step can take a long time and may require additional steps to remove impurities. The method is also not highly sensitive, and needs a high concentration of sulfate ions, which poses another problem [30] because this concentration of sulfates can be quite low in attacked concrete. Furthermore, ICP is not capable of providing high-resolution sulfate profiles. Rather, it measures the concentration of sulfate in a small area of the sample. It may be necessary to make measurements at different depths, making the work quite tedious [10,13].

To assess the progress of sulfate attack, an alternative to measuring the width of the penetration front of sulfate ions is to measure the effects of the attack, such as ESA-induced expansion. Invar wire (wire with low thermal expansion and dimensional stability) can be used to monitor the expansion of an RC structure [31]. Invar wire must be anchored to the concrete to function properly. A properly anchored and secured wire is necessary for accurate measurement. A second challenge is reading and interpreting the invar wire readings. Environmental factors such as moisture, temperature, and mechanical stress may affect the measurements. Additionally, invar wire is not a real-time expansion tracking tool. The process of reading and recording measurements at regular intervals often requires manual intervention. This can be time-consuming and resource-intensive, and limits the ability to detect specific concrete problems in a timely manner [31].

On the other hand, artificial intelligence (AI) has the potential to revolutionize the measurement and assessment of expansion, damage, and crack appearance on concrete structures by leveraging advanced computational techniques for image analysis and pattern recognition [32]. In fact, AI algorithms, particularly deep learning models, can be trained to detect and analyze cracks in images of concrete structures with high accuracy and efficiency [33]. Based on the appearance, size, and orientation of cracks, these models can be trained to recognize and categorize different types of cracks. Additionally, it is possible to develop systems that can analyze image data in order to measure the expansion of concrete structures over time [34]. This type of system can provide quantitative measurements of structural changes by training AI models to identify specific markers of expansion, such as crack patterns and deformations in concrete. Despite AI's accelerated use in the construction field, it still requires improvement and its use is not always simple.

This article aims to propose two new techniques to evaluate the performance of cement paste specimens against ESA. The first method consists in observing the penetration depth of sulfate ions after a drying procedure. A comparison is made between the results obtained by this method and those obtained by ICP. The second method is to measure the changes in length caused by ESA-induced expansion with an optical fiber (OF). The feasibility and effectiveness of this method are then challenged by comparing the OF measurements with those obtained with a simple digital extensometer.

2. Materials and Methods

2.1. Materials

The cement paste used in this study was composed of CEM I 52,5 N CE CP2 NF with a water-to-cement ratio of 0.6. Cement composition and anhydrous content based on Bogue's equations are shown in Tables 1 and 2, respectively.

Table 1. Composition of cement CEM I 52.5 N CE CP2 NF provided by the manufacturer.

Components	wt %
CaO	62.79
SiO ₂	20.38
Al ₂ O ₃	4.30
TiO ₂	0.24
Fe ₂ O ₃	3.80
MgO	1.25
SO ₃	3.46
S	Traces
K ₂ O	0.73
Na ₂ O	0.35
Chlorides	0.04
MnO	0.05
LOI (loss on ignition)	2.04
Insoluble	0.54
Σ	99.97
Free lime	1.39

Table 2. Main cement clinker phases calculated by Bogue's equations.

Components	Mass Content Based on Bogue Equation %
C ₃ S	57.05
C ₂ S	14.99
C ₃ A	7.91
C ₄ AF	8.9

Cylindrical specimens were used for the first proposed method (i.e., the drying method developed to evaluate the penetration depth of sulfate ions). The cement paste specimens were cast in a rigid PVC mold with a diameter of 10 cm and a length of 15 cm (see Figure 1a). Plastic covers were attached to both ends of the mold. The purpose of using such molds was to reduce the risk of desiccation that might occur during the hydration process, particularly with high-water content pastes. Vibration was used to compact each layer of filling as it was poured into the molds during the casting process. Voids were eliminated as a result of this process.

To ensure that the cement paste cylinders were homogeneous and to avoid any separation of the solid particles and water, the cylinders were placed after casting in a large cylindrical device (see Figure 1b) and rotated at a low speed (1 cycle/min) for 16 h. A similar technique was used in [6,10].

One day after casting, 1 cm slices were removed from both sides of the cylinders to eliminate the edge effects, and to obtain a homogeneous paste in cylinders (see Figure 1c). Two identical cylindrical slices (length = 5 cm and diameter = 10 cm) were cut from each remaining cylinder (see Figure 1c). The specimens (slices) were intended to be immersed in an attack solution (see description of exposure conditions below). However, before immersion, each slice was coated on its lateral surface with epoxy resin (see Figure 1d) and allowed to cure for 24 h. With this type of protection, the sulfate ions present in the immersion solution are only allowed to penetrate into the cement paste through the bottom circular base of the cylindrical slice (the upper part of the slice is out of the solution as explained in the description of exposure conditions below).

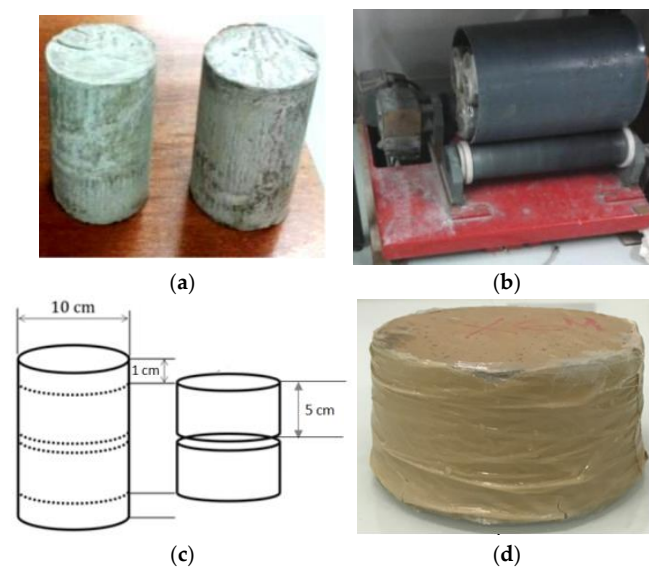


Figure 1. Sample preparation: (a) cement paste cylinders obtained after casting; (b) rotation device used to treat the cylinders and avoid bleeding; (c) cylinder cutting; and (d) coated specimen.

2.2. Sampling and Exposure Conditions

After one month of curing in water, the specimens were immersed (to a depth of 1 cm) for a period of 24 weeks in a solution of Na_2SO_4 at a concentration of 15 g per liter, which was demonstrated by several studies to be the most appropriate for ESA testing [10,11]. The immersion depth of the specimens was only 1 cm, corresponding to a partial immersion usually referred to as semi-immersion. The rest of the sample depth (4 cm) was exposed to air. The test solution was maintained at a pH of 8, which is believed to be representative of field exposure conditions, especially in the case of partially immersed RC structures.

As part of the acceleration method, it is necessary to maintain pH at 8 (± 0.1), and so the set-up shown in Figure 2 was developed and used with a titration system injecting sulfuric acid (H_2SO_4) solution at 0.02 M. This technique ensures that the sulfate ion concentration remains approximately constant throughout the entire experiment. The specimens were exposed in baths connected to a central underside bath with a capacity of 80 L where the titration was performed. In the central bath, a 750 L per hour pump delivers the solution to the exposure baths at the same concentration and flow rate as the central bath. An additional supply of sulfate ions was provided by renewing the solution every two weeks. Detailed information about the developed device can be found in [10].

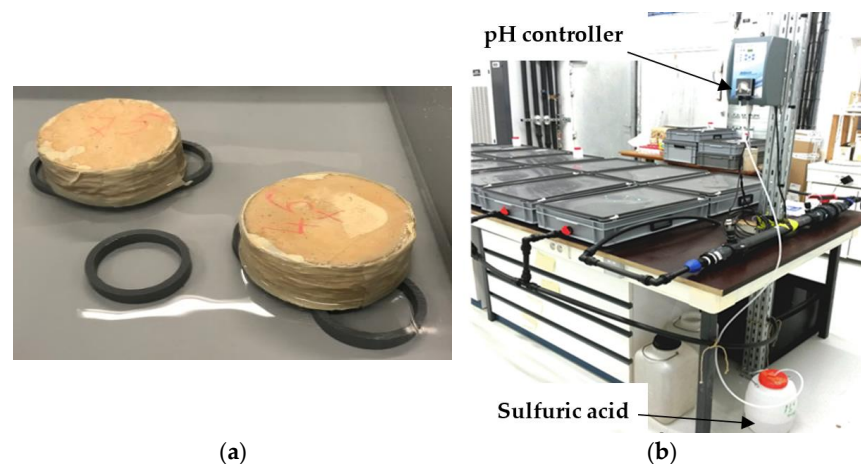


Figure 2. (a) Semi-immersion exposure; (b) photo of the pH-control device developed in the laboratory and used for this study.

2.3. Test Method for Evaluating the Penetration Depth of Sulfate Ions

As previously discussed, the first method presented in this article aims to evaluate the penetration depth of sulfate ions into cement paste samples. In this experimental work, salt precipitation was observed at the following intervals over a period of 24 weeks: 2, 4, 6, 8, 12, 16, and 24 weeks. The time periods were not chosen randomly. A preliminary study utilizing the ICP technique was conducted using the same formulations used in this work, which allowed us to apply the same drying times. There was a breakdown of the samples during the last period of time (24 weeks), which explains why the final period of time was chosen for the experiment.

During the semi-immersion of the cylindrical specimens in the sulfate solution, sulfate ions are forced to move upward from the immersed portion of the specimen to the outer surface as a result of the capillary rise mechanism in semi-immersion [35].

For each time interval, one 5 cm long cylinder was removed from the Na_2SO_4 solution and cut in half (see Figure 3a,b) to obtain two parts that were placed in a climatic chamber at 50% RH and $T = 20^\circ\text{C}$ for two to three hours. Then, salt crystallized on the surfaces exposed by the cut when the supersaturated solution evaporated from this newly air-exposed part of the specimen, resulting in the precipitation of white particles [36]. The formed white surface corresponds to the zone of crystallization of free sodium sulfate crystals (Na_2SO_4) due to evaporation conditions [37]. Under specific temperature and relative humidity conditions, the precipitate is caused by crystallization of thenardite (Na_2SO_4) and mirabilite ($\text{Na}_2\text{SO}_4 \cdot 10\text{H}_2\text{O}$) under high concentrations of Na_2SO_4 solution [38,39]. This white zone should be examined in the future via SEM-EDX (scanning electron microscopy with energy-dispersive X-ray analysis) in order to identify all the phases that formed there.

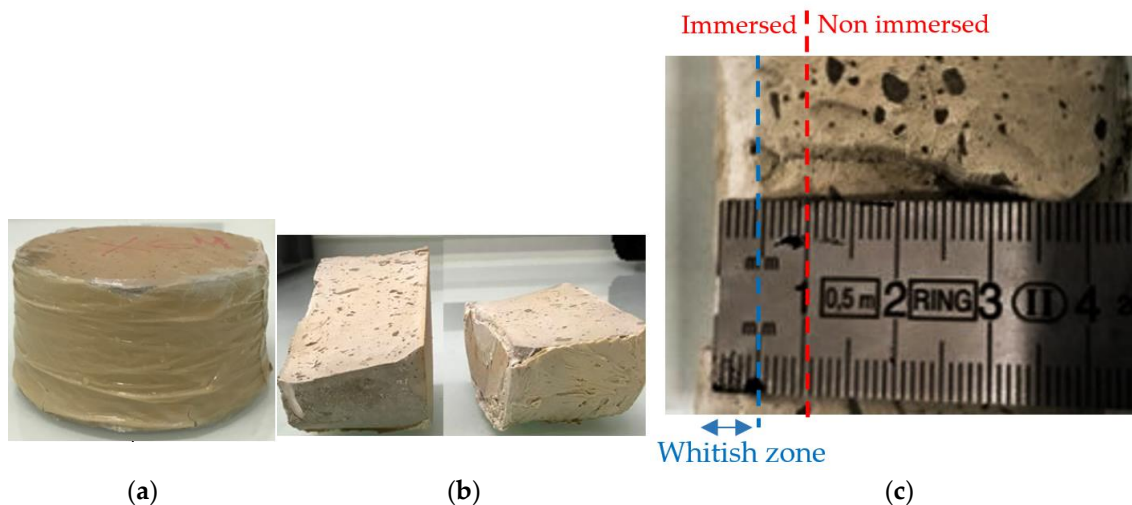


Figure 3. The two stages of preparation of the cement paste specimen and the measurement of the penetration depth: (a) sample removed from bath; (b) specimen cut in half before being placed in a climatic chamber at 50% RH and $T = 20^\circ\text{C}$; (c) white precipitation measured with a stainless-steel ruler.

Finally, the width of the whitish precipitate zone was measured with a stainless-steel ruler at the end of the drying phase (see Figure 3c).

2.4. Optical Fiber-Based and Extensometer Methods for Measurement of ESA-Induced Expansion

The second method presented in this article aims to measure ESA-induced expansion using an optical fiber-based method. To perform this monitoring, three cement paste prismatic specimens ($3 \times 4 \times 16 \text{ cm}^3$) were cast with the CEM I 52.5 N CE CP2 NF at a water-to-cement ratio of 0.6. Figure 4a shows fresh cement paste poured into a mold common to three specimens. Each prism was crossed by a fiber embedded along its length. The location of the OF in each prism is detailed in Figure 4b. The outer parts of the OF

were protected by a plastic sheath. A pair of stainless-steel pins was bonded to one side of each prism, allowing an extensometer to be used to measure expansion. The side of the prism equipped with the pair of pins was the side closest to the OF. The pins are bonded to the specimens with a strong chemical adhesive that is resistant to chemical attacks in solutions such as sulfate solution. There is a small hole at the top of the pins, which matches the extensometer pointers and the reference length bar (Figure 4c). A generating line was formed by aligning each pair of pins in the center axis of the prism at an initial length of 100 mm (see Figure 4d).

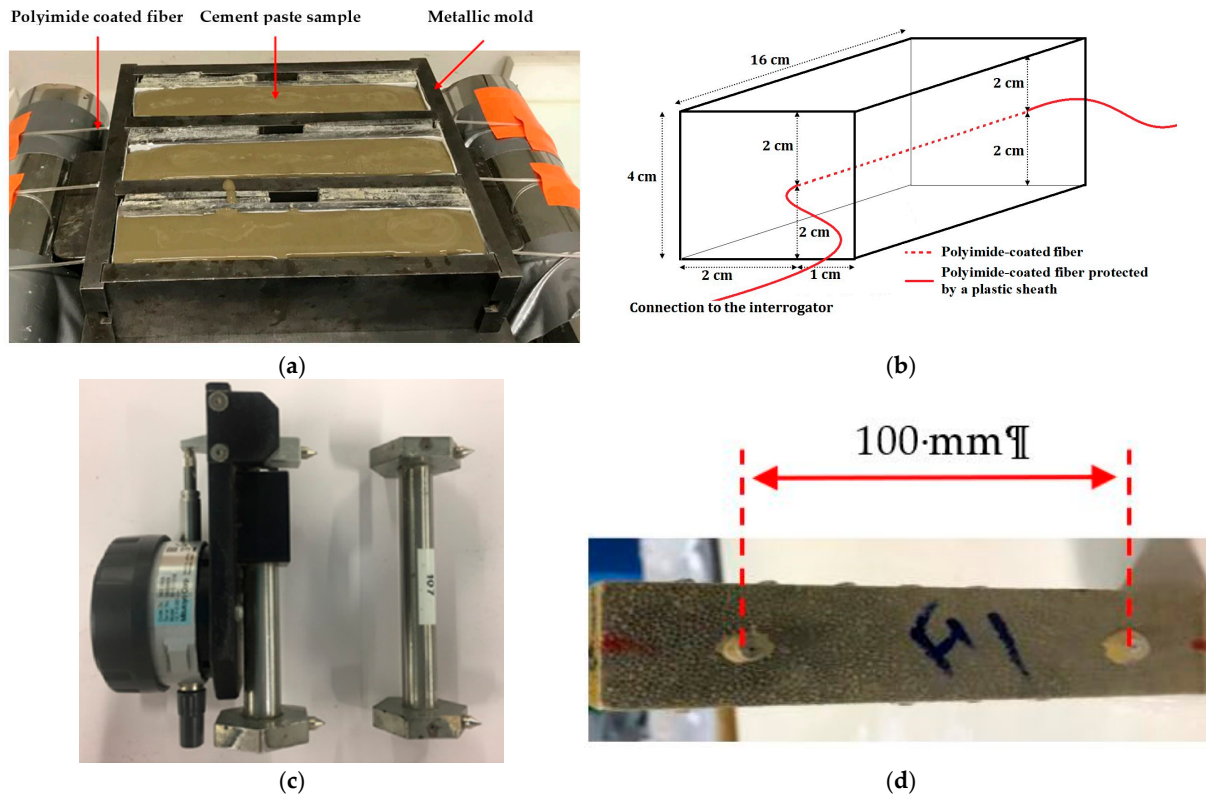


Figure 4. Experimental set-up: (a) cement paste just cast in the metallic mold; (b) geometry of cement paste prismatic specimen equipped with OF; (c) extensometer (left) and reference length bar (right); (d) cement paste prism equipped with a pair of pins.

Immediately after demolding, the prisms were placed in water to cure for 30 days. Then, the prisms were immersed in a 15 g/L Na_2SO_4 solution to induce ESA. Expansions were then recorded, at different time intervals of the exposure, using a Rayleigh backscattering-based interrogation device [40,41]. This device can give information about material expansion by measuring the changes in the frequency of the backscattered light caused by the stress-induced strain within the material. This technique, known as distributed fiber optic sensing, allows for the detection and monitoring of structural expansion. To apply this technique, a coherent light source, such as a laser, is launched into one end of an optical fiber. As the light travels through the fiber, a small fraction of it interacts with the material and is scattered back along the fiber in the opposite direction.

Using optical fibers for the measurement of deformations offers several advantages over the use of invar wire. Optical fibers provide higher accuracy and sensitivity, allowing for precise measurements of small deformations. The precision of this technique enables measurements in the range of micrometers or even nanometers. Additionally, optical fibers are nonconductive and immune to electromagnetic interference, making them suitable for a wide range of environments. They also offer the capability for distributed sensing, enabling

the measurement of multiple points along the fiber. Moreover, using fiber optic sensors provides a nonintrusive monitoring solution.

When the material or structure undergoes deformation (expansion in the case of ESA), it induces strain on the optical fiber. This strain causes a change in the optical properties of the fiber, such as the wavelength or intensity of the light propagating through it. This change is then detected by the optical sensing system. The optical signal captured by the sensing system is processed to extract the relevant information related to the deformation. This may involve using a demodulation unit to convert the optical signal to an electrical signal that can be further analyzed to determine the magnitude and distribution of the deformation. This analysis involves comparing the optical signal after deformation of the instrumented sample/structure with a reference signal (before deformation), using algorithms to interpret the changes in the signal, and spatially resolving the deformation along the length of the optical fiber.

3. Results

3.1. Visual Inspections

At different time intervals (up to 24 weeks), the macroscopic degradation of cement paste specimens was observed during the ESA. The main stages of this degradation are as follows:

- After 12 weeks of exposure, a circumferential crack appeared at the exposed edge of the immersed base of the specimens (see Figure 5a).
- After 20 weeks, the cracks grew wider and larger, moving from the edges towards the center. Then the cylinders started to exhibit clearly visible crack patterns and began to lose their cohesion (Figure 5b).
- After 24 weeks, there was a significant deterioration of the cylinder at its immersed edge (see Figure 5c). At the periphery of the bottom base (immersed and not protected by epoxy), there was substantial damage and loss of cohesion, while at the center of this base, there were no visible signs of damage.



Figure 5. Degradation of cement paste due to ESA: (a) after 12 weeks; (b) after 20 weeks; (c) after 24 weeks.

It can be concluded that the expansion is more significant in the saturated portion of the semi-immersed sample (in contact with the Na_2SO_4 solution), which results in significant tensile stresses near the periphery (see Figure 5). These observations are comparable to those obtained by [10] from the side and front. During ESA, significant tensile stresses developed near the surface, resulting in this particular cracking pattern characterized by the appearance of orthoradial macrocracks and the deterioration of peripheral areas. The entire degradation process can be explained by the crystallization pressure theory, which states that the crystals must form from an oversaturated solution in order to generate the energy necessary for expansion. It is also crucial that the crystals precipitate in small pore spaces so that the stress generated by expansion is greater than the tensile strength of the material [10].

During this experimental work, the ESA-induced expansion was not monitored. However, the visual macroscopic deformations suffered by the cement paste samples confirm the primary role of expansion in the degradation process (cracks appeared and propagated where the specimen deformed the most). It is notable that the observed deformation shape was consistent with the results of a calculation based on the model developed at Gustave Eiffel University, based on a thermodynamic approach to describe the formation of crystals inside porous mediums [42,43] to re-evaluate the structural damage caused by internal sulfate attack (ISA). Despite the fact that each type of sulfate attack has a specific physicochemical mechanism, Gustave Eiffel's model helped to predict qualitatively the deformation of the studied specimens subjected to ESA.

As the modeling was not intended to be quantitative, it is not described here. Nevertheless, it is worth pointing out that the considered geometry of the samples and boundary conditions were all consistent with the experiments. Details of the modeling can be found in [44].

In line with the numerical prediction of swelling (Figure 6a), circumferential cracks were experimentally observed at the surface of the portion exposed to the attacking solution (see Figure 6b,c).

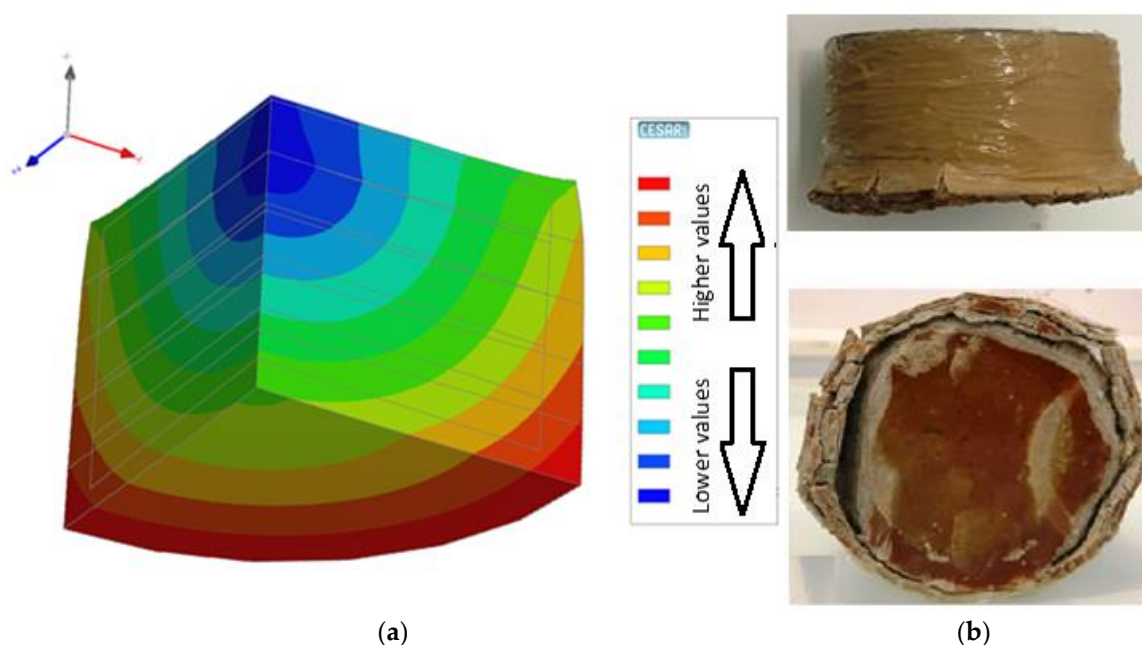


Figure 6. (a) ISO values of the displacement field predicted by the FE model; (b) visual appearances of the cement paste cylindrical samples after 24 weeks of exposure to ESA.

3.2. Sulfate Profiles

As part of this study, the penetration front of sulfate ions into cement pastes was investigated by visually inspecting the formation of white, fine, and powdery precipitates to determine the depth of the attacked zone. At each scheduled time (2, 4, 6, 8, 12, 16, and 24 weeks), a specimen was removed from the attacking solution, cut in half, and placed in a climatic chamber. Photos of the two cut surfaces were then taken. The visualizations are based on images analyzed using optical microscopy. The contrast of the images was enhanced to improve the visibility of the attacked zone (Figure 7). In each specimen, the width of the attacked zone was calculated as the average value of seven values measured at seven locations of the attacked zone. All the values obtained at the different measurement dates were then used to plot the time evolution of the attacking front (Figure 8).

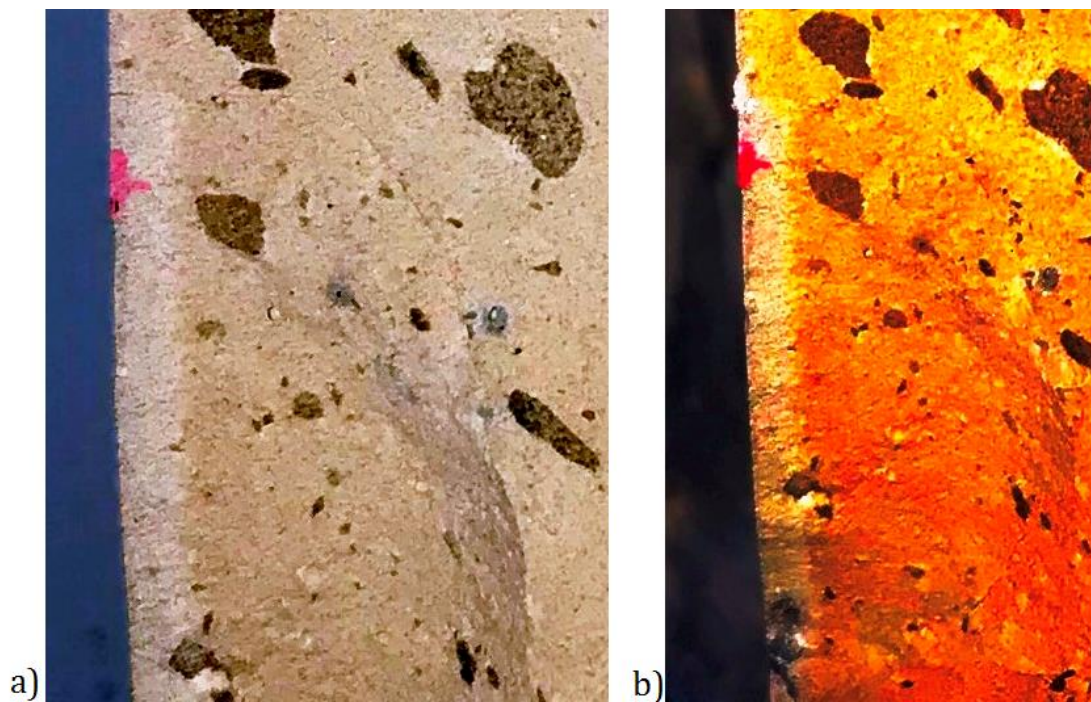


Figure 7. (a) White precipitation obtained by drying method; (b) photo with enhanced contrasts.

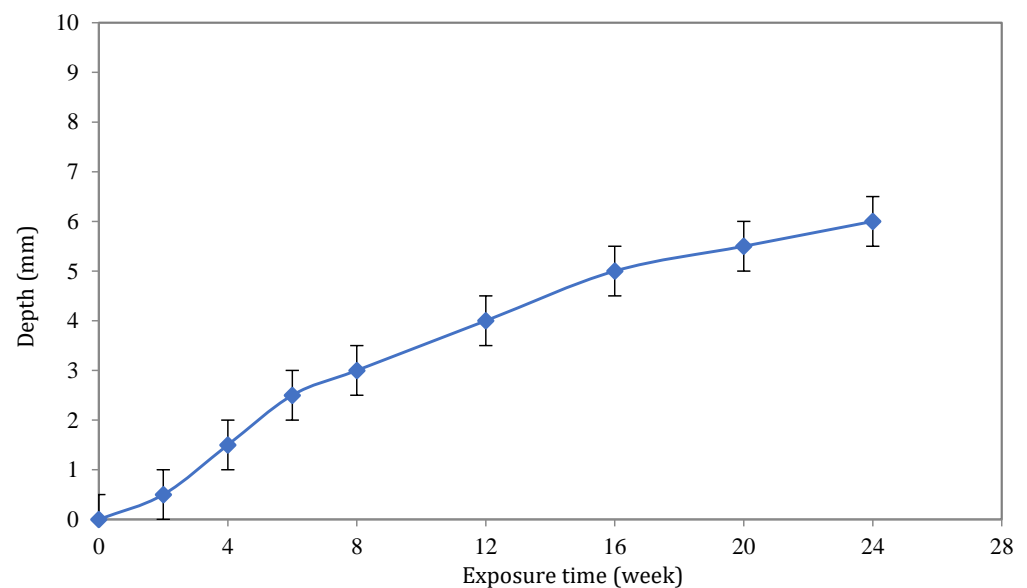


Figure 8. Penetration depth of sulfate ions measured by the drying method for 24 weeks.

In order to confirm that the white precipitation area in the attack zone was indeed precipitated sulfate, Raman tests were conducted on both affected and non-affected zones. The results of the tests confirmed that the precipitated product in the attack zone was indeed precipitated sulfate (Figure 9). Indeed, this figure shows two patterns for sulfate-affected and non-affected zones. The two patterns are quite similar, except for a peak around 980 cm^{-1} . This is identified as a characteristic peak associated with sulfate ions. It corresponds to the symmetric stretching vibration of the sulfur–oxygen bonds in the sulfate ions.

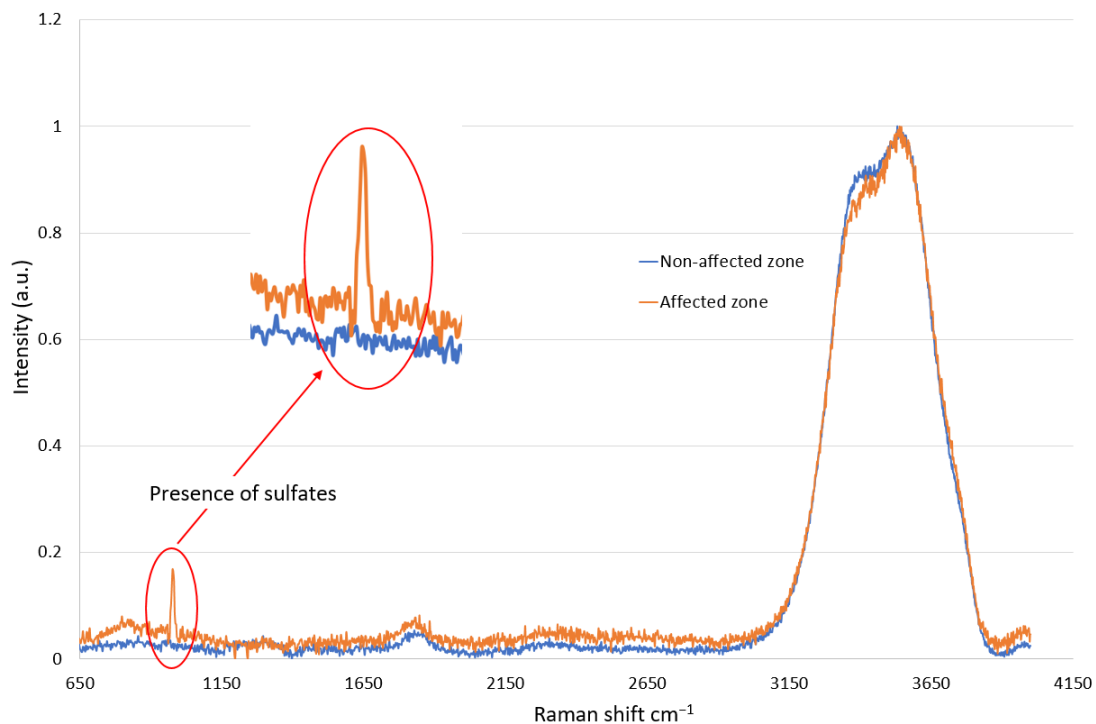


Figure 9. Sulfate signal in the affected zone of the sample.

To challenge the proposed method, a comparison was made between the penetration depth measured by this drying method and the sulfate penetration results obtained using the inductively coupled plasma atomic emission spectroscopy (ICP-AES) method. This comparison was made between the profiles of sulfate penetration obtained by Ragoug et al. in a previous research project using the ICP-AES technique [10]. In the present study, the exposure conditions related to the work of Ragoug et al. were reproduced in order to ensure that the results obtained by the proposed investigation method and those obtained by ICP-AES are highly comparable. In the ICP method, a sample is prepared and subjected to acid to extract the sulfates. The resulting solution is then analyzed using ICP spectrometry, which involves the generation of high-temperature plasma to atomize and ionize the sample. The ionized atoms are then quantified based on their unique emission or absorption spectra, allowing for the precise measurement of sulfate concentrations in different layers of the sample.

With the ICP-AES method, the total sulfur concentration ($[\text{SO}_3]$ weight percent in g/g of anhydrous cement) can be determined in cement paste samples, resulting in the quantification of the sulfate content. The specimens were ground from their exposed surfaces (bottom circular bases) to a depth of 12 mm. At each grinding step, the amount of powder corresponds to a 1 mm thick sample and contains an average particle size of 315 microns. The extracted powder contains sulfates that have been ionized by an acid attack. After the solution was prepared, it was analyzed using an ICP-AES instrument. Due to the laborious aspect of ICP analysis, only one ICP measurement was performed by measurement time and by considered depth.

It should be noted that although the proposed technique (i.e., drying technique) allows a quantitative evaluation of the penetration depth of the attack by ESA, it is not able to measure the sulfate content that is associated with each penetration depth. On the contrary, the ICP-AES analysis can provide a detailed description of the penetration profile. An example of the penetration profiles measured during the study of Ragoug et al. is shown in Figure 10. More detailed information regarding the procedure for obtaining sulfate profiles by ICP-AES can be found in [10].

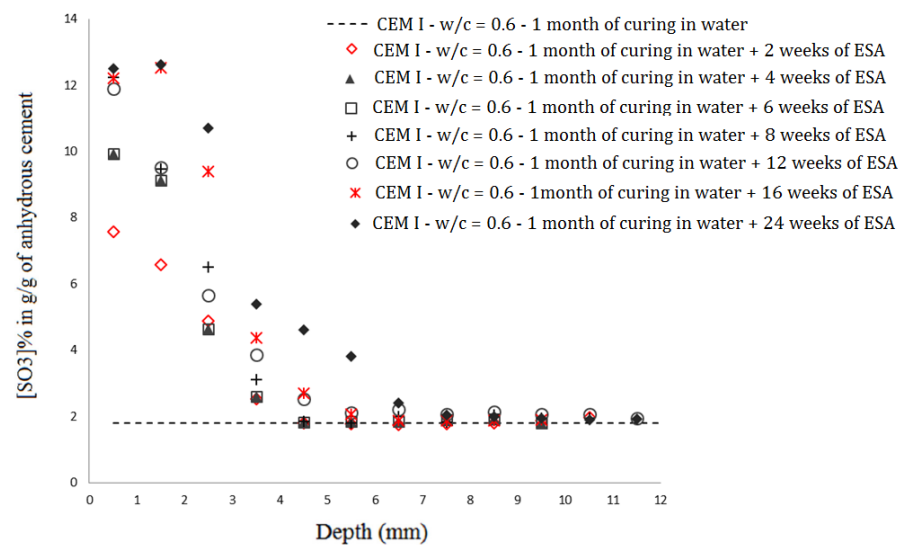


Figure 10. Sulfate profiles measured by ICP-AES for different exposure durations to ESA (from [45]).

It is important to note that sulfate ions are transferred to the cement matrix during the process of ESA, and calcium ions are leached to the outer solution during the process. It is a two-mode process, one involving diffusion, which is considered to be the dominant phenomenon, and the other involving the physicochemical fixation of sulfate ions in the cement matrix [10]. Sulfate ions penetrate materials more slowly when the concentration difference between the inside and outside of the material is reduced. This case shows an accumulation of sulfate ions on the surface of the samples. This means that sulfates detected through the drying procedure correspond to those remaining in the interstitial porous solution that crystallized under applied evaporation conditions ($T = 20\text{ }^{\circ}\text{C}$ and $\text{RH} = 50\%$).

The sulfate profiles measured by ICP-AES are presented in Figure 10. These profiles were considered in order to obtain the values of the penetration front depth to be compared with those obtained by the drying method. In Figure 10, the black dashed line illustrates the initial content of sulfate in sound cement paste (of the order of 2% in g/g of anhydrous cement). Considering this initial presence of sulfate, the depth value deduced for each exposure period is the highest depth value of the corresponding profile (in the X axis) for which the concentration of SO_3 is bigger than the initial value. It must be underlined that, in the ICP-AES method, sulfate concentrations were calculated from the total sulfur concentration ($[\text{SO}_3]$ % in g/g of anhydrous cement). As a consequence, the sulfate content measured by ICP-AES is more similar to the solid phase content, which includes the total sulfates present in the matrix (free sulfates and combined sulfates).

Figure 11 illustrates the comparison between the results obtained by the ICP-AES and drying methods. By comparing the penetration depths obtained by drying and ICP-AES, it is apparent that both techniques permit us to describe the evolution of the penetration front of sulfate. According to ICP-AES, the highest depth recorded by the method was 6.5 mm, whereas the highest depth recorded by drying was 5 mm. Compared with the results obtained by the drying method, which revealed only free sulfate contributions, the ICP-AES results were higher due to the significant sulfate content in the solid phase, which was physically and chemically combined. This contributed to the higher depths obtained by ICP-AES compared with those obtained by the drying method. Despite the differences in results between the two methods, we note a similar trend in the curves, particularly after 8 weeks of exposure to the sulfate solution. This suggests that there is a relationship between the results of the two techniques and that a coefficient should be proposed to switch between them. It can be concluded that the drying method is suitable for expert cases because of its ease of use compared with the ICP technique.

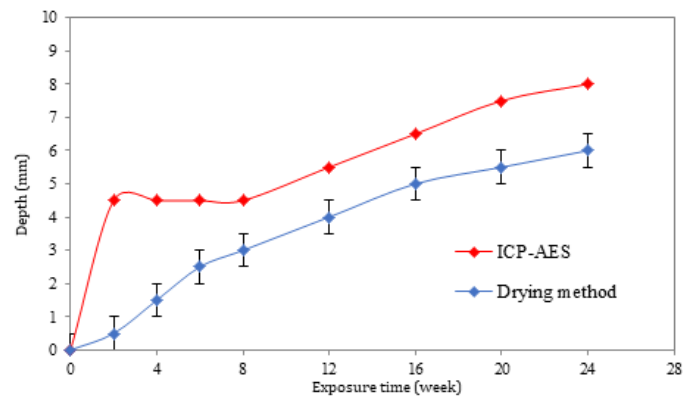


Figure 11. Penetration depth of sulfate ions measured by ICP-AES and drying method after 24 weeks of semi-immersion in the Na_2SO_4 solution.

Some parameters, such as type of binder, w/c, and curing period, may influence the definition of the white precipitation zone. The type of binder used in a material can influence the definition of a white precipitation zone due to its chemical composition, reactivity, and interactions with other elements present in the material. Different binders, such as Portland cement, slag, or fly ash, have distinct hydration behaviors and produce varying reaction products. The lower the portlandite content, the less this white precipitation zone appears. Moreover, a higher w/c ratio may contribute to increased leaching of soluble alkalis and calcium hydroxide, leading to the formation of efflorescence or white precipitates on the material surface as water evaporates. This can impact the detection of the white zone caused by sulfate precipitation. Finally, extended curing periods can promote the formation of crystalline compounds, affect the degree of hydration, and potentially alter the solubility and migration of ions within the material, which could impact the appearance and definition of the white precipitation zone. The drying conditions applied play a major role and should be optimized according to the parameters listed (w/c ratio, type and content of SCM, curing duration).

3.3. ESA-Induced Expansion Measurement Using Optical Fibers

To determine if optical fibers could be used to measure ESA-induced expansion, the three cement paste prisms whose fabrication is described in Section 2.4 were fully immersed in sodium sulfate solution for 100 days. Figures 12 and 13 show the results of the expansion as measured by the extensometer and by the embedded OF, respectively. As an initial remark, it can be indicated that these figures illustrate the highly repeatable expansion behavior of the specimens.

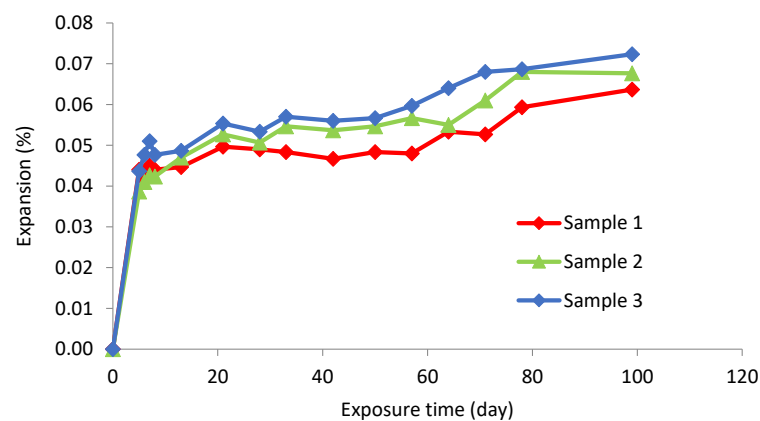


Figure 12. Evolution of ESA-induced expansion measured with extensometer.

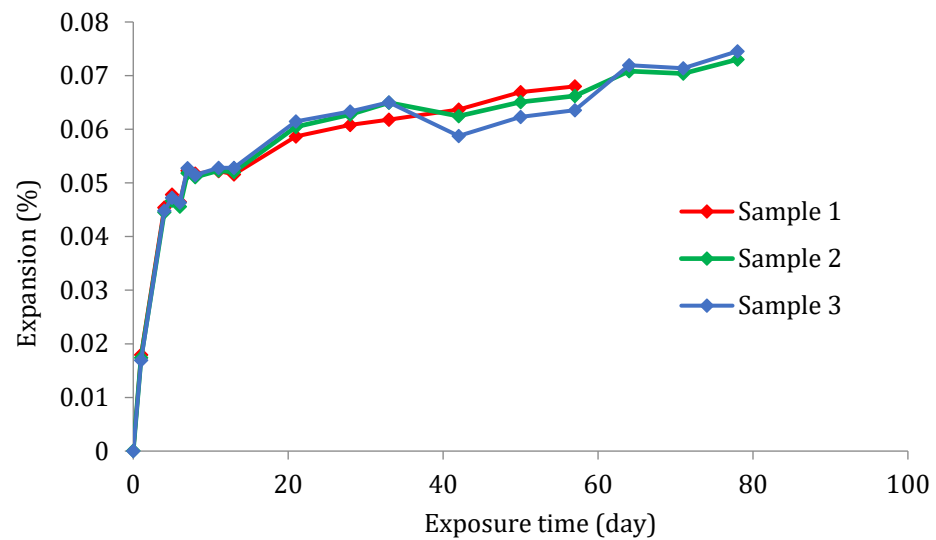


Figure 13. Evolution of ESA-induced expansion measured with OF.

The averaged measurement results for each sensor type are shown in Figure 14. This allows the validity of the results obtained with the OF sensors to be assessed, as extensometer measurement is considered to be a widely proven technique. As shown in Figure 14, the OF measurements were satisfactorily similar to those obtained with an extensometer, although the optical fibers measure slightly higher deformations. For example, the average final expansion recorded with the extensometers (before rupture of OF sensors) was 0.065%, while that recorded with the OF was 0.074%. Furthermore, the expansion paths were nearly identical regardless of the measurement method used.

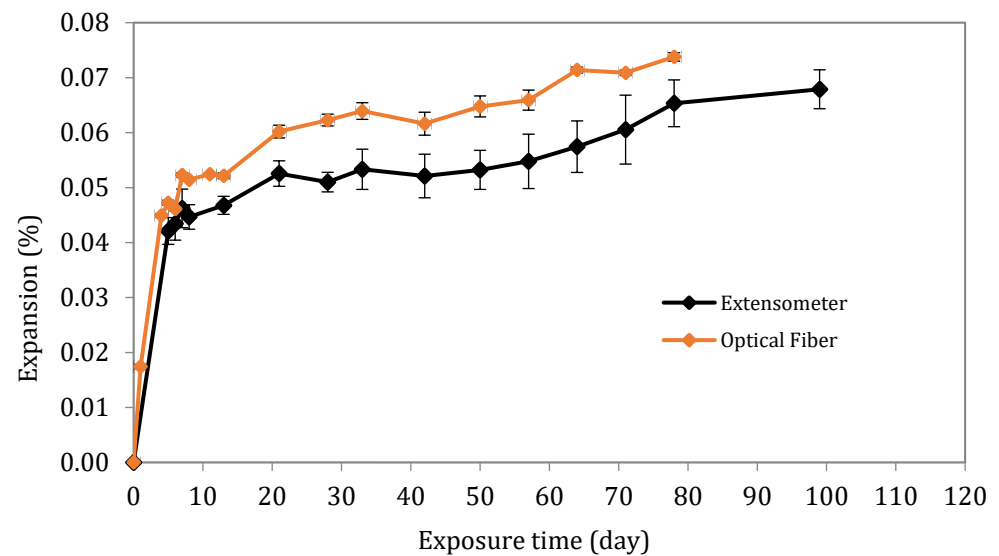


Figure 14. Comparison of ESA-induced expansion measured with OF or with extensometer.

The first OF failure occurred after 57 days of immersion of the specimens (the OF of sample 1 in Figure 13). The two remaining OFs failed a few days after the last measurement (78 days of immersion) for unknown reasons (chemical attack on the coating and/or mechanical damage due to frequent handling of the extensometer during the measurement).

4. Discussion

4.1. Discussion Regarding the Drying Method

Based on the results of the described study, the proposed method for assessing the depth of the affected zone due to ESA appeared to be quite effective. As a result of the aggressive evaporation conditions imposed in the procedure ($T = 20\text{ }^{\circ}\text{C}$ and $\text{RH} = 50\%$), sodium sulfate crystallized inside the material, creating a sort of white precipitate on the surface exposed by the cut of the specimen. It should be noted that even though the quantitative results obtained by the drying method differed from those obtained by ICP-AES, the same trends and slopes were observed for both methods, particularly after 8 weeks of exposure. The observed differences are explained by the fact that ICP-AES takes into account all of the total sulfur concentration (free and combined sulfates) while sulfate content examined by the drying method represents the number of free sulfates remaining in the interstitial solution.

By using the proposed method, time can be saved and measurements can be taken without prior thorough preparation. Moreover, the results are easily obtained and interpreted within a few minutes owing to the use of a simple steel ruler. As an alternative, the quantitative determination of the affected depth using ICP-AES requires many hours of meticulous preparation while respecting and following very specific procedures.

Also, it should be noted that the quantitative identification of the penetration front of sulfate ions by the drying method appears to be applicable in situ to assess the depth of the sulfate front in a real RC structure. An evaluation of this type can be carried out by coring a sample and then allowing the curved lateral surface to dry by air.

However, the drying method is not as accurate as ICP-AES. Also, due to the dark texture of the binders usually used in sulfate-resisting cements (like CEM III and CEM V), it could be difficult to detect visible white precipitates in the drying surface. As a final note, the primary concern with the drying method is that it detects only free sulfates that are present in the cement matrix's interstitial solution.

Several aspects should be considered in future works to complete and improve the technique presented in this section. For example, the images obtained after drying could be processed and analyzed using a specific image analysis software. In the presented work, image contrast processing was performed in a very simple way using basic software, and depth measurement was performed manually, whereas software could have provided a depth measurement based on contrast analysis.

In addition, a colored indicator that reacts with sulfate ions can help detect whitish precipitates. Lastly, it is possible to optimize the treatment conditions (RH and temperature) in order to enhance their effects and to obtain a more visible contrast between the cement paste and the attacked area.

Using simple assessment techniques to determine the extent of ESA has several advantages over more complex chemical methods. It is worth noting that simple assessment techniques are generally less expensive and easier to implement, allowing preliminary results to be obtained quickly. Furthermore, these simple assessment techniques can be used in the field to facilitate the inspection of structures and to provide real-time assessment. In this way, areas affected by ESA can be quickly identified, and appropriate preventive or corrective action can be taken. However, even though the proposed simple assessment technique can provide preliminary and indicative results regarding sulfate penetration in concrete structures, it is not as accurate as more complex chemical methods. Therefore, it may be necessary to use more advanced chemical techniques to accurately assess the progress of the ESA attack. These techniques may include the following: (i) aluminum nuclear magnetic resonance (Al NMR) and X-ray diffraction (XRD) tests to quantify ettringite produced during the ESA chemical process, (ii) thermogravimetric analysis (TGA) tests to quantify portlandite consumed to form secondary ettringite, (iii) scanning electron microscopy (SEM) tests to determine if the sulfate penetration front has occurred, and (iv) mercury intrusion porosimetry (MIP) tests to identify microstructure changes.

4.2. Discussion Regarding ESA-Induced Expansion Measurement Using Optical Fibers

The second experimental technique investigated in this paper is the use of OF sensors to measure ESA-induced expansion of laboratory specimens. For this application, the optical fibers do not require any special conditioning but only need to be implanted in the mold prior to casting the specimen. During the experiments, the expansion measurements obtained using OF sensors were comparable to those obtained using the traditional method (extensometer). As a result of this comparison, it can be concluded that OF-based techniques are able to follow the evolution of ESA-induced expansion. OF-based methods can then be considered as an alternative to measure ESA-induced expansion, thus providing insight into the behavior of cement-based materials.

In fact, the proposed technique offers significant advantages, despite the fact that OF installation is more complicated than gluing the pins. A major perspective (not tested here) is to automate measurements on a very large number of prisms and at many different timescales, whereas monitoring with an extensometer would require a great deal of work. This could, for example, make it possible to monitor automatically, at the same time, series of specimens manufactured with different formulation parameters (different cements, different cement blends, different water-to-cement ratios, etc.).

It is notable that in the present study, the only type of optical fiber tested (polyimide-coated OF) was damaged after 57 or 78 days of exposure to the Na_2SO_4 solution due to uncertain reasons. In light of the above, one of the major improvements that can be considered for future studies is to test other coatings of OFs. In future validation investigations of OFs with other coatings, a set of samples equipped only with OFs and a set of specimens equipped only with stainless-steel pins will be considered in order to eliminate the risk of damaging the OFs during measurement with the extensometer.

5. Conclusions

Two new test methods were introduced in this paper to study the ESA at the scale of cement paste specimens. First, sulfate ion penetration depth measurements were performed on cylindrical specimens after imposing drying conditions on their cut surfaces. Second, OF sensors were used to monitor the ESA-induced expansion of cement paste prisms.

The results of the proposed drying method were compared with the sulfate ion penetration depths obtained by ICP-AES to determine the reliability of the proposed method. Two comparable and parallel paths were then observed in terms of penetration depths, especially considering the results obtained after 8 weeks of accelerated ESA. However, the ICP-AES curve maintained a higher amplitude than the drying method. This is attributed to the fact that ICP-AES is able to detect both chemical and physical sulfates, whereas drying only quantifies free sulfates. In future investigations, the white precipitate should be examined via SEM-EDX to identify all the phases that have formed there. It would also be beneficial to include other types of cement and different exposure conditions in future studies to obtain more information on the efficiency of this method compared with the traditional ICP-AES method.

By using advanced techniques for analyzing images of sample surfaces and identifying sulfate profiles, artificial intelligence and image analysis methods can be used for the measurement of ESA profiles in the material. High-resolution images can be captured and analyzed using image analysis software. Artificial intelligence algorithms may be trained to recognize and extract key features associated with ESA, such as ettringite formation, gypsum deposits, and other indicators of sulfate attack. Furthermore, AI algorithms can learn to recognize patterns and characteristics specific to ESAs through the use of machine learning models. In this way, the system can automatically identify areas of the concrete surface that have been affected by sulfate attack before or after the appearance of the damage. This technique can then classify different levels of ESA severity and quantify the extent of damage in the material. In addition to providing valuable insights into the progression of sulfate attack, this type of quantitative information can also be used to assess the structural integrity of concrete.

An optical fiber-based method was also developed to monitor the changes in length of cement paste samples as a result of ESA-induced expansion. The measurements were compared with those obtained using a conventional extensometer. After exposure to accelerated ESA, both techniques recorded almost the same expansion evolution and final average expansion (about 0.07%). This result confirms that ESA-induced expansion can be accurately monitored with OF sensors. Due to the deterioration of the optical fiber, the exposure lasted for only 78 days, which is a sufficient duration for some test methods, such as Swiss standard SN 505262-3 [46]. This suggests that future studies should continue this experimental work by testing other types of OF. In any case, the proposed method has great potential, for example as a means of automatically monitoring a large number of samples.

Author Contributions: Validation, conceptualization, methodology, and writing—review and editing, O.O.M., M.Q., M.J. and V.B.-B.; writing—original draft preparation, investigation, and formal analysis, O.O.M. and M.Q.; supervision, O.O.M., M.Q. and V.B.-B. All authors have read and agreed to the published version of the manuscript.

Funding: This research received no external funding.

Institutional Review Board Statement: Not applicable.

Informed Consent Statement: Not applicable.

Data Availability Statement: Data are contained within the article.

Conflicts of Interest: The authors declare no conflicts of interest.

References

1. Scrivener, K.; John, V.M.; Gartner, E.M. Eco-efficient cements: Potential economically viable solutions for a low-CO₂ cement-based materials industry. *Cem. Concr. Res.* **2018**, *114*, 2–26. [[CrossRef](#)]
2. Habert, G.; Espinosa, A.; Roussel, N. Economic and environmental impact of Portland cement substitution by industrial by-products: A life-cycle assessment application in France. *Resour. Conserv. Recycl.* **2011**, *57*, 48–57.
3. Scrivener, K.L.; Martirena, F.; Bishnoi, S. Alternative clinkers. *Cem. Concr. Res.* **2018**, *114*, 27–39.
4. Xu, W.; Li, H.; Maruyama, I. Energy efficiency and CO₂ emission reduction opportunities in the cement industry in China. *Energy* **2017**, *141*, 1466–1475.
5. Hooper, D.; Woodward, D. Fiber Bragg Grating Sensors in Civil Infrastructure: A Review. *IEEE Sens. J.* **2019**, *19*, 9011–9024.
6. Yingwu, Z.; Hao, T.; Lili, S.; Feng, X.; Ningxu, H. Strength Deterioration of Concrete in Sulfate Environment: An Experimental Study and Theoretical Modeling. *Adv. Mater. Sci. Eng.* **2015**, *13*, 951209.
7. Menéndez, E.; García-Rovés, R.; Aldea, B.; Salem, Y. Review of the Incidence of the Sulphate Attack in Spain. Evaluation of Field Concrete Cases. In *External Sulphate Attack—Field Aspects and Lab Tests*; RILEM Bookserie; Menéndez, E., Baroghel-Bouny, V., Eds.; Springer: Cham, Switzerland, 2020; Volume 21. [[CrossRef](#)]
8. Benkaddour, M.; Kenai, S.; Yahiaoui, W.; Bensaci, H.; Khatib, J. Rheological, mechanical and durability performance of some North African commercial binary and ternary cements. *Case Stud. Constr. Mater.* **2023**, *19*, e02689. [[CrossRef](#)]
9. Amine, Y.; Leklou, N.; Amiri, O. Effect of supplementary cementitious materials (scm) on delayed ettringite formation in heat-cured concretes. *Energy Procedia* **2017**, *139*, 565–570. [[CrossRef](#)]
10. Ragoug, R.; Metalssi, O.O.; Barberon, F.; Torrenti, J.M.; Roussel, N.; Divet, L.; de Lacaillerie, J.B.D.E. Durability of cement pastes exposed to external sulfate attack and leaching: Physical and chemical aspects. *Cem. Concr. Res.* **2019**, *116*, 134–145. [[CrossRef](#)]
11. El Inaty, F.; Marchetti, M.; Quiertant, M.; Omikrine Metalssi, O. Chemical Mechanisms Involved in the Coupled Attack of Sulfate and Chloride Ions on Low-Carbon Cementitious Materials: An In-Depth Study. *Appl. Sci.* **2023**, *13*, 11729. [[CrossRef](#)]
12. Yin, G.J.; Wen, X.D.; Miao, L.; Cui, D.; Zuo, X.B.; Tang, Y.J. A Review on the Transport-Chemo-Mechanical Behavior in Concrete under External Sulfate Attack. *Coatings* **2023**, *13*, 174. [[CrossRef](#)]
13. Thomas, P.; Ramu, Y.K.; Martin, L.; Vessalas, K.; Sirivivatnanon, V. Assessment of the Potential for Delayed Ettringite Formation in Heat Cured Mortars and Concrete Using Australian Materials. *Constr. Mater.* **2023**, *3*, 529–542. [[CrossRef](#)]
14. Falaciński, P.; Machowska, A.; Szarek, Ł. The Impact of Chloride and Sulphate Aggressiveness on the Microstructure and Phase Composition of Fly Ash-Slag Mortar. *Materials* **2021**, *14*, 4430. [[CrossRef](#)] [[PubMed](#)]
15. Whittaker, M.; Black, L. Current knowledge of external sulfate attack. *Adv. Cem. Res.* **2015**, *27*, 532–545. [[CrossRef](#)]
16. Irassar, E.F. Sulfate attack on cementitious materials containing limestone filler—A review. *Cem. Concr. Res.* **2009**, *39*, 241–254. [[CrossRef](#)]
17. Wang, K.; Guo, J.; Yang, L.; Zhang, P.; Xu, H. Multiphysical damage characteristics of concrete exposed to external sulfate attack: Elucidating effect of drying–wetting cycles. *Constr. Build. Mater.* **2022**, *329*, 127143. [[CrossRef](#)]

18. Zhong, C.; Huang, B. Deterioration Process of Cementitious Material Properties under Internal Sulphate Attack. *Appl. Sci.* **2023**, *13*, 3982. [[CrossRef](#)]
19. Liu, Y.; Li, W.; Guan, J.; Zhou, X.; Guo, L. Fully coupled peridynamic model for analyzing the chemo-diffusion-mechanical behavior of sulfate attack in concrete. *Constr. Build. Mater.* **2023**, *409*, 133874. [[CrossRef](#)]
20. Tixier, R.; Mobasher, B. Modeling of damage in cement-based materials subjected to external sulfate attack. II: Comparison with experiments. *J. Mater. Civ. Eng.* **2003**, *15*, 314–322. [[CrossRef](#)]
21. Zhang, M.; Qin, S.; Lyu, H.; Chen, C.; Zou, D.; Zhou, A.; Li, Y.; Liu, T. A transport-chemical-physical-mechanical model for concrete subjected to external sulfate attack and drying-wetting cycles. *Eng. Fract. Mech.* **2023**, *293*, 109726. [[CrossRef](#)]
22. Zhang, Z.; Zhou, J.; Yang, J.; Zou, Y.; Wang, Z. Understanding of the deterioration characteristic of concrete exposed to external sulfate attack: Insight into mesoscopic pore structures. *Constr. Build. Mater.* **2020**, *260*, 119932. [[CrossRef](#)]
23. Ikumi, T.; Segura, I. Numerical assessment of external sulfate attack in concrete structures. A review. *Cem. Concr. Res.* **2019**, *121*, 91–105. [[CrossRef](#)]
24. Ejbouh, A.; Ech-chebab, A.; Hassi, S.; Galai, H.; Ebn Touhami, M. Durability assessment of LC3-based reinforced concrete under combined chloride-sulfate environment via the EIS technique. *Constr. Build. Mater.* **2023**, *366*, 130194. [[CrossRef](#)]
25. Kowalska, M.; Grzesik, B.; Adamczyk, Z.; Nowak, J.; Konsek, A. Swelling of sulfate-bearing soil: A case study of A1 highway pavement failure. *Case Stud. Constr. Mater.* **2023**, *18*, e02081. [[CrossRef](#)]
26. Zhang, Z.; Jin, X.; Luo, W. Long-term behaviors of concrete under low-concentration sulfate attack subjected to natural variation of environmental climate conditions. *Cem. Concr. Res.* **2019**, *116*, 217–230. [[CrossRef](#)]
27. Taheri, S. A review on five key sensors for monitoring of concrete structures. *Constr. Build. Mater.* **2019**, *204*, 492–509. [[CrossRef](#)]
28. Al-Nehmi, A.J.A. Assessment of Chloride and Sulfate Concentrations in Concrete Using Laser-Induced Breakdown Spectroscopy (LIBS). Ph.D. Thesis, King Fahd University of Petroleum and Minerals, Dhahran, Saudi Arabia, 2012.
29. De Weerd, K.; Justnes, H.; Geiker, M.R. Changes in the phase assemblage of concrete exposed to sea water. *Cem. Concr. Compos.* **2014**, *47*, 53–63. [[CrossRef](#)]
30. Houk, R.S.; Thompson, J.J. Inductively coupled plasma mass spectrometry. *Mass Spectrom. Rev.* **1988**, *7*, 425–461. [[CrossRef](#)]
31. Lohonyai, A.J.; Korany, Y.; Gül, M. Remote field monitoring of thermal and moisture deformations in masonry cavity wall building envelopes. *J. Perform. Constr. Facil.* **2015**, *29*, 4014072. [[CrossRef](#)]
32. Laxman, K.C.; Tabassum, N.; Ai, L.; Cole, C.; Paul Ziehl, P. Automated crack detection and crack depth prediction for reinforced concrete structures using deep learning. *Constr. Build. Mater.* **2023**, *370*, 130709. [[CrossRef](#)]
33. Li, R.; Yu, J.; Li, F.; Yang, R.; Wang, Y.; Peng, Z. Automatic bridge crack detection using Unmanned aerial vehicle and Faster R-CNN. *Constr. Build. Mater.* **2023**, *362*, 129659. [[CrossRef](#)]
34. Kuchipudi, S.T.; Debduitta, G. Automated detection and segmentation of internal defects in reinforced concrete using deep learning on ultrasonic images. *Constr. Build. Mater.* **2024**, *411*, 134491. [[CrossRef](#)]
35. Chen, F.; Gao, J.; Qi, B.; Shen, D. Deterioration mechanism of plain and blended cement mortars partially exposed to sulfate attack. *Constr. Build. Mater.* **2017**, *154*, 849–856. [[CrossRef](#)]
36. Rodriguez-Navarro, C.; Doehne, E.; Sebastian, E. How does sodium sulfate crystallize? Implications for the decay and testing of building materials. *Cem. Concr. Res.* **2000**, *30*, 1527–1534. [[CrossRef](#)]
37. Bassuoni, M.T.; Nehdi, M.L. Durability of self-consolidating concrete to sulfate attack under combined cyclic environments and flexural loading. *Cem. Concr. Res.* **2009**, *39*, 206–226. [[CrossRef](#)]
38. Tsui, N.; Flatt, R.; Scherer, G. Crystallization damage by sodium sulfate. *J. Cult. Herit.* **2003**, *4*, 109–115. [[CrossRef](#)]
39. Müllauer, W.; Beddoe, R.E.; Heinz, D. Sulfate attack expansion mechanisms. *Cem. Concr. Res.* **2013**, *52*, 208–215. [[CrossRef](#)]
40. Henault, J.-M.; Quiertant, M.; Delepine-Lesoille, S.; Salin, J.; Moreau, G.; Taillade, F.; Benzarti, K. Quantitative strain measurement and crack detection in RC structures using a truly distributed fiber optic sensing system. *Constr. Build. Mater.* **2012**, *37*, 916–923. [[CrossRef](#)]
41. Rolland, A.; Quiertant, M.; Khadour, A.; Chataigner, S.; Benzarti, K.; Argoul, P. Experimental investigations on the bond behavior between concrete and FRP reinforcing bars. *Constr. Build. Mater.* **2018**, *173*, 136–148. [[CrossRef](#)]
42. Omikrine Metalssi, O.; Kchakech, B.; Lavaud, S.; Godart, B. A new model for the analysis of the structural/mechanical performance of concrete structures affected by DEF—Case study of an existing viaduct. *Struct. Concr.* **2016**, *17*, 1104–1113. [[CrossRef](#)]
43. Martin, R.-P.; Omikrine Metalssi, O.; Toutlemonde, F. Importance of considering the coupling between transfer properties, alkali leaching and expansion in the modelling of concrete beams affected by internal swelling reactions. *Constr. Build. Mater.* **2013**, *49*, 23–30. [[CrossRef](#)]
44. Jabbour, M. Multi-Scale Study of the External Sulphate Attack in Reinforced Concrete Structures. Ph.D. Thesis, Gustave Eiffel University, Champs-sur-Marne, France, 2019.

45. Ragoug, R. External Sulphate Attack of Cementitious Materials: Impact of Different Age Factors, Binder Composition, Chloride Presence. Ph.D. Thesis, Gustave Eiffel University, Champs-sur-Marne, France, 2016.
46. Jabbour, M.; Metalssi, O.O.; Quiertant, M.; Baroghel-Bouny, V. A Critical Review of Existing Test-Methods for External Sulfate Attack. *Materials* **2022**, *15*, 7554. [[CrossRef](#)] [[PubMed](#)]

Disclaimer/Publisher's Note: The statements, opinions and data contained in all publications are solely those of the individual author(s) and contributor(s) and not of MDPI and/or the editor(s). MDPI and/or the editor(s) disclaim responsibility for any injury to people or property resulting from any ideas, methods, instructions or products referred to in the content.